Influence of steam dilution on the ignition of hydrogen, syngas and natural gas blends at elevated pressures

N. Donohoe[a], K.A. Heufer[a], C. J. Aul[b], E. L. Petersen[b], G. Bourque[c], R. Gordon[c], H.J. Curran[a,1]

[a]*Combustion Chemistry Centre, NUIG, University Road, Galway, Ireland*
[b]*Department of Mechanical Engineering, Texas A&M University, College Station, TX, USA*
[c]*Rolls-Royce Canada, Montreal, Canada*

Abstract

This paper presents the influence of steam dilution on the autoignition behaviour of hydrogen, carbon monoxide, syngas, methane, and natural gas mixtures under gas turbine-relevant conditions. Rapid compression machine experiments were performed for fuel/air mixtures at equivalence ratios of 0.5, 1.0, and 2.0, in the temperature range 895–1140 K for the H_2 and CO mixtures and 730–1060 K for the natural gas mixtures and at pressures of 10 and 30 bar. Shock-tube experiments were performed for CH_4-O_2-Argon mixtures with and without H_2O addition, highly diluted in argon (98% by vol.). The parameters were varied using an L9 Taguchi matrix for equivalence ratios of 0.5, 1.0, and 2.0; pressures of 1.6, 11, and 30 atm; and water contents of 0, 10, and 30% of the fuel by volume. It was found that significant changes in the thermal properties of the mixtures affect the reactivity, whereas no chemical effect of the steam addition was observed for the majority of the mixtures investigated. Only mixtures of pure carbon monoxide were strongly influenced by water addition. In this case, the presence of water in the mixture allows the formation of relatively reactive ȮH radicals which enhances the possible oxidation chemistry of carbon monoxide leading to a greater observed reactivity of CO in the presence of water.

Keywords:

Hydrogen, Ignition delay times, Rapid Compression Machine, Natural gas, Syngas, Steam

[1] address: Combustion Chemistry Centre, School of Chemistry, NUI Galway, Ireland. Phone: 00353-91-493856. Email: henry.curran@nuigalway.ie URL: http://c3.nuigalway.ie/ (H.J. Curran)

Preprint submitted to Combustion and Flame April 29, 2013

Introduction

Gas turbines are playing an increasingly important role in the generation of electricity. Their simple design, fuel versatility, and overall efficiency has allowed for their widespread implementation in electrical power generation. Gas turbines are also tolerant of a wide range of fuels and are now functioning satisfactorily using natural gas [1], gasified coal [2], and renewable energy sources such as hydrogen and syngas [3]. Hydrogen is expected to play an increasingly important role as a clean energy carrier in industry. But, in the short-term the cheapest and the most viable option for producing hydrogen with low CO_2 emissions is to use fossil fuels with carbon capture and storage (CCS) [4]. This option has become increasingly important in power generation due to expanding awareness of environmental issues such as the production of SOx, NOx [5] and CO_2 [6] and the continuing abundance of natural gas and coal reserves [7]. In the last decade, power-generating combined-cycle power plants have increased in overall efficiency. Improvements have afforded an increase in thermal efficiency to about 60% [8], while NOx emissions have been reduced by an order of magnitude, to below 9 ppm (dry, at 15% O_2) in some cases [9]. For the near future, there appears to be no alternative other than to use fossil fuels for large-scale power generation. Continuous research into renewable fuels and increasing turbine efficiency are needed.

Research into increasing gas turbine efficiency has yielded some promising technologies. The combined-cycle power plant is now well established and offers superior performance to any of the competing systems which are likely to be available in the medium term for large-scale power generation applications [10]. Integrated Gasification Combined Cycle (IGCC) power plants with Carbon Capture and Storage (CSS) have become increasingly attractive for notable greenhouse emissions reduction and the ability to use coal and syngas as well as natural gas as fuel sources [11]. IGCC is a type of power technology particularly favourable for carbon dioxide capture as the CO_2 can be removed at a convenient stage of the process where its partial pressure is high [11]. This approach is attractive as coal feedstocks are expected to last longer than those of natural gas, and syngas is a renewable energy source. ASUs (Air Separation Units) also play a key role in improving the efficiency, availability, and operability of oxygen-fed IGCC power plants. The use of CCS can typically reduce power plant CO_2 emissions by around 85–95% [12]. An optimal integration between the ASU and the balance of the plant, especially the gasifier and the gas turbine, has significant potential for enhancing the overall plant efficiency.

Plant efficiency can also be improved by the use of heat recovery systems. Energy recovery from the exhaust gases and the generation of steam from processes such as Steam Injected Gas Turbines (STIG) are a normal practice to boost power in many applications. This process is a natural development of steam injection in regenerative cycles, which consists of a gas turbine combined with a Heat Recovery Steam Generator (HRSG) [13]. The steam used for injection is produced from fresh water in a HRSG by cooling the hot exhaust gases from the gas turbine. The steam is then supplied before or in the combustion chamber or at the turbine inlet. The flue gases and steam expand in the turbine and thereafter heat new water.

Steam injection has been shown to improve thermal efficiency and reduce NOx emissions. Air from the compressor and steam from the HRSG both receive fuel energy in the combustion chamber and both expand inside the same turbine to boost the power output of the turbine. The specific heat of superheated steam is almost double the value of air and the enthalpy of steam is higher than that of air at relevant temperatures [13]. Therefore, the STIG method is a very effective way to boost the net power output and increase the overall efficiency of gas turbines [14].

To investigate the effect of steam on the fuel combustion behavior, studies need to be performed using various gas turbine-related fuels with steam addition. Moist hydrogen experiments have been performed previously in rapid compression machines [15], compression ignition engines [16], and shock tubes [17]; moist methane and hydrogen have also been investigated in jet-stirred reactors [18]. However, to the authors' knowledge, a broad and in-depth ignition delay time study of steam addition to hydrogen, syngas, and natural gas mixtures has not been investigated. Consequently the aim of this study was to investigate the influence of steam on the ignition of hydrogen/CO and natural gas mixtures under turbine-relevant conditions. Experiments in a rapid compression machine and in a shock tube and simulations with a recent C_0–C_5 kinetic mechanism were used to analyse the effect of water addition on the autoignition behavior of these mixtures.

This paper details the results of the experiment and modelling study to examine the effect of water addition on the ignition chemistry of the target syngas, methane, and natural gas fuel blends. Presented first are the descriptions of the rapid compression machine and shock-tube experiments and related procedures, along with the mixtures that were studied. A description of the kinetic model and calculation approach is then given, followed by the experimental results and discussion. This last section begins with a model prediction study, followed by the results of the hydrogen experiments, the methane experiments, the natural gas tests, and CO experiments.

Experimental details

Rapid Compression Machine

Experiments were performed in the Rapid Compression Machine (RCM) facility at the National University of Ireland Galway (NUIG). This machine has a horizontally opposed, twin-piston design that has been described in previous studies [19, 20]. The pistons are tightly sealed inside two compression sleeves that adjoin the reaction chamber [21]. The symmetry of the device helps to reduce the aerodynamic effects inside the combustion chamber at the end of the compression process. By the opposed movement of two twin pistons, compression times below 16 ms are achieved. The diameter of the reaction chamber is 38.2 mm, and special care has been taken to ensure a homogenous pre-heating of the reaction chamber is possible up to 160°C. A large drive chamber is positioned behind each piston and serves as a reservoir of compressed air which is used to drive the pistons in place prior to compression. A hydraulic locking mechanism holds the pistons in place prior to compression. A hydraulic

stopping mechanism brings the pistons to a complete stop at the end of compression. Creviced piston heads have been designed to reduce the formation of roll up vortices and boundary layer effects. By using flat piston heads, the cooler gases from the wall mix with the adiabatic reacting core and results in a non-uniform temperature distribution. Since the chemistry is very sensitive to temperature this makes interpretations and modeling very problematic [21]. With the addition of creviced pistons, boundary layer effects are negligible, and the reacting core is temperature-homogeneous and adiabatic.

Gas mixtures have been prepared in separate stainless steel mixing vessels with a minimum mixing time of 2 hours before use. Table 1 presents an overview of the mixtures investigated. In each case, the oxygen/diluents ratio was 21/79, and a mixture of 50% nitrogen and 50% argon was used as the diluent. Only in the case of mixtures C1 and C2 was 100% argon used in the experiment to reach higher temperatures. Each mixture was investigated at 10 and 30 bar. A list of all the experimental data taken over the course of this study can be found in the supplementary material.

The ignition delay time (τ) for the RCM tests was defined as the time from the end of compression, taken as the time of peak compressed pressure, to the onset of ignition, Fig. 1. As well as reactive experiments, non-reactive experiments where the oxygen content was replaced by nitrogen were also performed for each condition. From the pressure profiles obtained from these experiments, volume profiles have been deduced assuming isentropic compression/expansion. These volume profiles are used in kinetic simulations to account for facility effects, i.e. the change in pressure and temperature during compression and after the end of compression due to heat loss effects. The validity of this methodology has been shown in previous studies [19, 20].

Special care has been taken to obtain the correct pressure profiles in the non-reactive experiment. The pressure transducer (Kistler 603B) used in this study is not heat shock resistant, i.e. the rapid temperature increase of the gas in the reaction chamber during compression and the resulting heat loads to the transducer respectively lower the output signal of the transducer. To prevent this effect from influencing the accuracy of the pressure measurement, the pressure transducer has been covered by a thin silicone layer in the non-reactive experiments. This layer acts to shield the sensor against the heat load during the experiment. From these experiments, the correct compression ratio and pressure profile were determined. The reactive experiments were performed without the silicone layer since it can interfere with the chemical reactions under investigation, influencing the reactivity and leading to spurious ignition delay time measurements. The temperature at end of compression in the reactive experiments was derived using the compression ratio determined in the corresponding non-reactive experiments.

Figure 2 shows the effect of the thermal protection layer. The measured pressure in the comparative experiments is lower without the silicone thermal protection. Since the temperature profile is deduced from the pressure profile, then the temperature would also

be lower than reality using the profiles from the non-shielded sensor. This artificially lower temperature would result in longer ignition delay times in the simulation compared to simulation using the profile measured with the shielded sensor. Furthermore, the temperature at the end of compression would be lower using the end-of-compression pressure of the non-shielded sensor. Thus, this method reduces uncertainties in the temperature of the experiment and simulation. Similar observations have been reported in shock-tube studies [22]. In this case, the pressure gradient behind the reflected shock wave measured without a thermal protection layer on top of the pressure transducer is initially correct but displays a slight decay in the measured pressure at times after the reflected-shock passage. Nevertheless, since in rapid compression machine experiments no high natural sensor frequencies are required, heat shock resistant sensors with natural frequencies lower than the Kistler 603B could be used to avoid heat loads influencing the pressure measurement.

All gas mixtures for the RCM were prepared manometrically in stainless steel tanks with high purity gases (= 99.9%). For each experiment, a pressure profile and the piston positions were recorded on a digital oscilloscope. The pressure profile was recorded by the previously mentioned pressure transducer (Kistler 603B). The experimental compressed temperature, T_C, and the compressed pressure, p_C, were calculated using the initial temperature, T_i, and pressure, p_i, of the experiment, and the compression ratio was calculated from the non-reactive experiment. Calculations assumed adiabatic compression and frozen chemistry. These calculations were carried out using Gaseq [23] which considers the temperature and the mixture composition dependence of the heat capacity in equation (1):

$$\frac{\ln Pc}{Pi} = \int_{Ti}^{Tc} \frac{\gamma}{\gamma - 1} \frac{dT}{T} \qquad (1)$$

Uncertainty analysis of the complete experimental procedure showed possible deviation for the end of compression pressure p_C of ±0.5 bar and an uncertainty in the end of compression temperature T_C of ±5 K.

Shock Tube

All of the shock-tube experiments were performed using one of the high-pressure shock tube facilities at Texas A&M University (TAMU), described in more detail by Aul et al. [24]. The entire shock tube is made out of 304 stainless steel; the driver section has an internal diameter of 7.62 cm and a length of 2.46 m, and the driven section has an internal diameter of 15.24 cm with a 4.72-m length. A high-vacuum system was used to pump down the test section to pressures less than 10^{-5} Torr between each experiment. Conditions behind the reflected shock wave were calculated using the 1-D normal shock relations and the Sandia thermodynamic database [25] from the measured incident shock wave velocity as follows. Five piezoelectronic pressure transducers (PCB 113A) are located at known intervals along the driven section, providing four intervals from which to measure the incident-shock speed using Fluke PM-6666 time-interval counters. The resulting axial shock velocity profile is

extrapolated to the endwall to produce the shock speed at reflection. This procedure has been shown to produce reflected-shock temperatures to within 10–15 K [26].

Shock-tube experiments were performed to observe the effects of the addition of water on the ignition delay times of a baseline methane-oxygen mixture highly diluted in argon at various conditions. The test parameters were a combination of 3 equivalence ratios (0.5, 1.0, and 2.0), 3 pressures (1.6, 11, and 30 atm), and 3 amounts of water as a mole percentage of the CH_4 (0, 10, and 30). An L9 Taguchi test matrix was populated and it resulted in 9 mixtures to cover the range of desired conditions. The 9 mixtures used in these experiments are shown in Table 2.

Ignition delay times were directly measured in the shock tube from the pressure and emission traces obtained from the experiments. Sample traces from an experiment are displayed in Fig. 3, which shows the signals from both the sidewall emission of OH* and the sidewall pressure transducer. As described in Petersen [27], for dilute mixtures where the ignition event is not evident in the pressure trace, sidewall determinations of ignition delay time are more accurate than endwall measurements of the same. All measurements were done from the sidewall station located 1.6 cm from the endwall. The pressure measurement was performed using a Kistler 603-B1 piezoelectric transducer located at the bottom of the tube. Chemiluminescence from OH* was detected through a sapphire window at the measurement location; this light was focused onto a Hamamatsu 1P21 PMT in a homemade housing after passing through a narrowband optical filter centred at 307 ± 10 nm.

As seen in Fig. 3, the ignition event is evident only in the OH* measurement, and the ignition delay time is defined herein as shown. Note that there is a slight increase in pressure around the reaction time. This increase was in addition to a slight (< 2%/ms) increase in test pressure due to boundary layer-induced facility effects [22]. For the experiments herein, the facility-related pressure increase led to a corresponding temperature increase that is typically less than the 10–15 K estimated overall uncertainty in reflected-shock temperature. For example, a 1540 K experiment with an ignition delay time near 1.5 ms would experience a temperature rise of about 14 K, a 1670 K test with an ignition delay time of about 1 ms would see a 10 K increase overall, and at 1820 K with an ignition delay time near 0.5 ms would see a rise of about 5 K. The overall uncertainty in ignition delay times from the shock-tube experiments (due mostly to temperature, mixture uncertainty, and identification of the ignition event) is estimated at 10%.

Kinetic simulation

Kinetic simulations have been performed using the 0-D reactor package in Chemkin-Pro [28]. As previously mentioned, volume profiles deduced from pressure measurements with non-reactive mixtures are used in the simulation to account for facility effects. Heat loss effects are modelled as virtual expansions which lead to a pressure decrease in the adiabatic core in the combustion chamber. By introducing the virtual volume profile, the constant-volume simulation is perturbed. Thus, the final pressure and temperature histories in the simulation result from the sum of the influence of the specified volume profile and the fuel chemistry.

The detailed chemical kinetic mechanism utilized in this work is under constant development and optimization at the Combustion Chemistry Centre [29]. It is based on the hierarchical nature of combustion mechanisms. The $H_2/CO/O_2$ sub-mechanism is based on the work of Ó Conaire *et al.* [30] with several significant updates based on recent experimental and kinetic data. The changes are partially described in Kéromnès *et al.* [31] and are fully detailed in a separate publication [32]. The C_1–C_3 sub mechanisms are based on earlier work [33, 34] with the most recent refinements described in Metcalfe *et al.* [35]. The chemistry of some important unsaturated species including 1,3-butadiene, propene and allene are taken from Laskin *et al.* [36], primarily based on the earlier work of Davis and law [37]. The butane and pentane sub-mechanisms are unchanged from Healy *et al.* [34].

Results and discussion

Model analysis

Prior to performing the experimental results, the possible influence of steam on the ignition delay time was analysed by kinetic predictions. The condition with only hydrogen as fuel 'in air' was chosen first for its discussion comparing both cases with and without initial water content. Looking at reactions that are influenced by water concentration, the reactions $\dot{H} + O_2 (+M) = H\dot{O}_2 (+M)$ and $H_2O_2 (+H_2O) = \dot{O}H + \dot{O}H (+H_2O)$ are the most sensitive to ignition delay times within the investigated regimes of pressures and temperatures. In both reactions, water is a collision partner and, due to its stronger interactions with $H\dot{O}_2$ and H_2O_2 arising from dipole-dipole interactions, hydrogen bonding etc., water is a more efficient collision partner (10 times higher in our model for $\dot{H} + O_2 (+M)$) compared to nitrogen, which features a much weaker dipole–induced-dipole interaction [38] which promotes both reactions. Nevertheless, sensitivity analysis of these reactions showed that $\dot{H} + O_2 (+M) = H\dot{O}_2 (+M)$ inhibits reactivity while the reaction $H_2O_2 (+H_2O) = \dot{O}H + \dot{O}H (+H_2O)$ promotes reactivity.

We have tested the effect on ignition delay time predictions to 70% H_2/30% H_2O and 70% NG/30% H_2O mixtures in air at 30 bar of changing the third body efficiencies of water in the reaction $\dot{H} + O_2 (+M) = H\dot{O}_2 (+M)$ to unity and removing the reaction $H_2O_2 (+H_2O) = \dot{O}H + \dot{O}H (+H_2O)$ from the mechanism and setting the third body efficiency of water in the reaction $H_2O_2 (+M) = \dot{O}H + \dot{O}H (+M)$ equal to unity. Reducing the efficiency of water in these reactions effectively lowers their rate. Fig. 4(a) shows the effect on the hydrogen/water mixture. Changing the efficiency of the reaction $\dot{H} + O_2 (+M) = H\dot{O}_2 (+M)$ to unity has a negligible effect at temperatures below approximately 1000 K, but above this there is a slight increase in the predicted reactivity, with the ignition delay time being 20% faster at 1100 K. This is due to the competition of this reaction with the main chain branching reaction $\dot{H} + O_2 = \ddot{O} + \dot{O}H$ leading to an enhanced reactivity when the rate of the reaction $\dot{H} + O_2 (+M) = H\dot{O}_2 (+M)$ is decreased.

Reducing the rate of the reactions $H_2O_2 (+H_2O) = \dot{O}H + \dot{O}H (+H_2O)$ / $H_2O_2 (+M) = \dot{O}H + \dot{O}H (+M)$ reduces reactivity by 40% at 800 K and this reduction decreases to 23% at 1100 K. Analysing the effect of changing the rate of both of these reactions simultaneously shows that at temperatures below approximately 1000 K the reaction $H_2O_2 (+M) = \dot{O}H + \dot{O}H (+M)$ is more important than $\dot{H} + O_2 (+M) = H\dot{O}_2 (+M)$ for the H_2/H_2O mixture. For the NG/H_2O

mixture, there is little influence of the $\dot{H} + O_2 (+M) = H\dot{O}_2 (+M)$ reaction with the main influence seen by changing the rate of the $H_2O_2 (+H_2O) = \dot{O}H + \dot{O}H (+H_2O)$ / $H_2O_2 (+M) = \dot{O}H + \dot{O}H (+M)$ reactions, Fig. 4(b). The effect is most pronounced in the temperature range 750–1000 K where the ignition delay time increases by approximately 10% throughout the range of temperature.

Besides the influence on reaction rates, the water concentration in the mixture affects the mixture properties, namely the heat capacity and species concentrations. To distinguish between the effect on reaction rates and mixture properties, different kinetic simulations have been performed. First, simulations of pure hydrogen in air at 30 bar and at an equivalence ratio (φ) of 1.0 without water were used as a reference. For the second simulation the initial water content has been treated as an inert component. For this calculation, an additional species 'water inert' was introduced into the kinetic model such that it is only an inert collider and it does not directly take part in any reaction but influences the gas mixture properties (heat capacity and species concentration) as a diluent. Finally, full simulations with water influencing the reaction rates demonstrate the effect of the initial water concentration on the reactivity of the mixture.

Figure 5 shows the results for the aforementioned simulations assuming constant-volume, adiabatic conditions. Compared to the reference case without water in which the ignition delay times was calculated to be 680 ms at 800 K and 435 μs at 1100 K, ignition delay times become approximately 12% longer (764 ms at 800 K and 489 μs at 1100 K) for inert water addition as is expected due to the dilution of mixtures, Fig. 5(a). In the case where water chemistry is allowed to influence reaction rates, the ignition delay times become somewhat shorter at lower temperatures when compared to both other cases, it being predicted to be 559 ms at 800 K and 487 μs at 1100 K. Thus, the addition of water to the initial mixture has a slight promoting effect on the reactivity of the mixture. Nevertheless, the overall influence of water addition is smaller than typical experimental uncertainties so that no significant changes in ignition delay times are expected to be observed experimentally. Similar to the hydrogen mixtures, the natural gas mixtures have been analysed accordingly. Since the overall water concentration in the mixture is less for these mixtures the effect of it is even smaller, Fig. 5(b). Here adding 'inert' water leads to longer ignition times of approximately 3% at 700 K (ignition times changes from 282 ms to 292 ms) and 5% 1100 K (from 1302 μs to 1365 μs), while simulating with 'reactive' water increases times by about 3% at 700 K (from 282 to 290 ms) and insignificantly at 1100 K (from 1302 μs to 1307 μs).

For hydrogen mixtures, the thermal diffusivity decreases for higher water concentrations (Table 3) leading to less heat loss and thus a lower temperature and pressure decrease (see Fig. 6). For natural gas mixtures, the changes in thermal properties are lower because the relative concentration of water is lower than for the hydrogen mixtures. This lower water concentration leads to a less pronounced effect of water addition on the thermal properties of the natural gas mixtures.

Hydrogen experiments (Mixtures H1–H2)

Figure 7 shows ignition delay times versus inverse temperature for all hydrogen experimental data in the RCM. The plot shows that ignition delay times decrease with increasing pressure, temperature and equivalence ratio. These experimental results are accurately captured by the chemical kinetic mechanism.

In order to determine the quantitative difference between the model and the experiment, all experimental data were fit to a polynomial expression and experimental ignition delay times were re-calculated using this correlation. At 10 bar and φ = 0.5 the model predicts ignition times that are approximately 10% slower than those measured experimentally at low temperature (970 K), whereas at higher temperatures (1015 K) the model is approximately 22% faster compared to experiment. For the 10 bar, φ = 1.0 data the model is generally slightly faster compared to experimental measurements; at low temperature (950 K) the model predicts ignition times approximately 14% faster than measured experimentally, whereas at higher temperatures (1000 K) the model is approximately 7% faster than the experimental measurement. For the 10 bar, φ = 2.0 data the model is overall faster compared to the experimental data, it being approximately 30% faster at 940 K decreasing to 3% faster at 977 K and becoming 18% slower at 990 K. Similar trends are observed for the 30 bar data where the model predicts ignition delay times that are approximately 20–30% faster compared to experiment.

Figure 8 details the effect of water addition on ignition times for hydrogen mixtures at 10 and 30 bar and at an equivalence ratio of 1.0. Results for all other conditions investigated can be found as Supplementary Material. The simulations agree well with the experimental data and accurately capture the experimental trends. For the pure hydrogen mixture at 10 bar the model predicts ignition delay times that are generally within 10% of those measured experimentally. For the hydrogen mixture diluted with water the model is on average, 20% faster compared to experimental measurements. For the pure hydrogen mixture at 30 bar the model is approximately 50% slower compared to experiment at low temperature (905 K). However, at higher temperatures faster ignition times of approximately 20% are predicted compared to experiment. For the hydrogen mixture diluted with water at 30 bar the model is generally in excellent agreement with the measured data, it being on average approximately 3% faster compared to experimental measurements. In contrast to the discussion above, experiments and simulations show a significant effect of water addition on the ignition delay time. These differences result from differences in the thermal properties of the gas mixture leading to different facility behaviour. Due to a reduced thermal diffusivity for the 70% H_2 + 30% H_2O mixture the pressure drop after the end of compression induced by heat loss effects is less than in the case of pure hydrogen (see Fig. 6). Since the ignition delay time is not only a function of the conditions at the end of compression but results from the whole temperature and pressure history, particularly associated with the phase after compression, a lesser decrease in pressure and temperature for the mixtures with water dilution leads to shorter ignition delay times as observed here experimentally. Thus, it can be concluded that the addition of water has no significant direct chemical effect on the ignition delay time as

discussed before. These results are consistent with Fig. 5, where we see that water addition is not predicted to affect ignition delay times for adiabatic calculations but does affect ignition times in the actual experiments (see supplementary material) due to its lower thermal diffusivity leading to lower heat losses and thus shorter measured ignition delay times.

Natural gas mixtures (N1–N3)

The experiments for the natural gas (NG2) mixture with water have been performed at pressures of 10 and 30 bar and equivalence ratios of 0.5, 1.0 and 2.0. The change in thermal properties is less severe for the natural gas mixtures compared to the hydrogen experiments which results in similar non-reactive profiles for the different water concentrations investigated (Fig. 9). Thus, a significant change in the ignition delay times with different water concentration is neither expected in the experiments nor in the simulations of the three natural gas mixtures.
Figure 10 details the effect of water addition on ignition delay times of natural gas at 10 and 30 bar, and for stoichiometric (φ = 1.0) mixtures. Results for all other conditions investigated can be found in the Supplementary data.

Overall, the agreement of the model simulations with the experimental data is reasonably good. In general, the model predicts ignition delay times that are 20–50% longer than those measured experimentally for all eight mixtures. The ignition delay times decrease with higher temperatures, pressures, and equivalence ratios. Nevertheless, at high pressures and especially at high equivalence ratios a discrepancy between the simulation and experimental data is observed at lower temperatures (700–800 K) particularly for rich mixtures. At these conditions, the experiments show a strong change in the reactivity compared to the high-temperature behavior. Although the simulation also predicts some change in reactivity in this temperature regime, the simulated ignition delay times are significantly longer than in the experiments. Previous studies have shown [34] that the mechanism employed here is capable of accurately describing the ignition behavior of the single components of the natural gas mixtures (methane, ethane, propane, *n*-butane, *n*-pentane) so that it is unknown so far why for their mixtures measured here the model fails to reproduce the experimental behavior. However, it can already be concluded that the observed discrepancy between the model and the experimental results is not the result of the water addition since experiments without any water in the initial mixture composition show the same behavior.

CO mixtures (C1–C3)

Since carbon monoxide is significantly less reactive compared to all other fuels investigated, a higher compression ratio was achieved through the use of larger piston heads, which in turn led to a lower compressed volume. This higher compression ratio together with the use of argon as a diluent gas was implemented to achieve temperatures at the end of compression allowing for the measurement of ignition delay times within the operational regime of the used facility in an effort to capture the reactivity of carbon monoxide. Nevertheless, pure CO (mixture C1) was not reactive enough to be investigated in the rapid compression machine and thus only simulation results are presented in the following discussion for this mixture.

Figure 11 compares the CO mixtures for 10 bar (black lines and symbols) and 30 bar (red lines and symbols) at φ = 1.0. As before, the simulations agree well with all available experimental data and additional experimental results can be found in the supplementary material. For the C2 mixture at 10 bar the model is almost 40% slower than the experimental data at 1080 K. At higher temperatures the model agrees with the data within less than 10%, and predicting ignition times that are 22% faster than the experimental measurements at 1130 K. For the C2 mixture at 30 atm the model is 86% slower than the experimental measurements at the lower temperature of 1025 K, but is within 10% of the experimental results throughout the remainder of the temperature range. For the C3 mixture at both 10 atm and 30 atm the model is slightly faster (within 20% at worst) than experiment at lower temperatures (890–950 K) and is slower by about 20% at the highest temperatures (960–1015 K). For all data sets, the ignition delay times decrease with increasing pressure and with temperature as is to be expected. A significant increase in reactivity is observed for the carbon monoxide with water addition when compared to the pure CO mixture. A further increase in reactivity is observed when 50% of the CO is replaced by hydrogen (35% H_2 + 35% CO + 30% H_2O mixture). For discussion of the significant differences in reactivity of the CO mixtures with and without water, a reaction pathway analysis has been performed at 30 bar, 1050 K and at φ = 1.0 (Fig. 12).

Initially the fuel can only react with O_2 producing CO_2 and an oxygen radical Ö (CO + O_2 = CO_2 + Ö). In the case without water in the initial mixture, this oxygen radical can only react with CO producing CO_2 (CO + Ö (+M) = CO_2 (+M)). However, with water present in the initial mixture the oxygen radical can react with water giving two ȮH radicals (Ö + H_2O = ȮH + ȮH). These ȮH radicals can react further with CO forming CO_2 and a hydrogen atom (CO + ȮH = CO_2 + Ḣ). The hydrogen atom can then react with O_2 producing an oxygen atom and another ȮH radical (Ḣ + O_2 = Ö + ȮH). Thus, the initial water content allows the formation of ȮH radicals which is not possible without water for pure CO mixtures. ȮH radicals are very reactive, resulting in a significantly higher reaction rate coefficient of CO + ȮH compared to CO + O_2 or CO + Ö. For this reason, the 70% CO + 30% H_2O mixture shows a significantly higher reactivity compared to pure carbon monoxide for all conditions investigated. For mixtures containing hydrogen, carbon monoxide, and water in the initial mixture composition, the hydrogen chemistry further increases the reactivity of the system leading to significantly shorter ignition delay times compared to the pure carbon monoxide mixture.

Comparison of all RCM mixtures

Figure 13 shows a general overview of the results of this study, where the RCM results for all mixtures at 30 bar and at an equivalence ratio of φ = 1 are plotted. More results are present in the Supplementary material. As discussed previously, the pure CO mixtures show the lowest reactivity due to the missing hydrogen chemistry pathways producing reactive OH radicals in contrast to the 70% CO + 30% H_2O mixture in the initial composition. Adding a sufficient amount of hydrogen to the mixture (35% CO + 35% H_2 + 30% H_2O) allows the hydrogen chemistry to dominate which further increases the reactivity compared to the CO mixture containing water [32].

The addition of water to the initial mixture composition has no significant chemical effect for mixtures which contain fuel species in addition to CO. None of these mixtures (H1–H2 and N1–N3) show a change of ignition delay times with varying water content. Comparing the hydrogen mixtures with the natural gas mixtures, the natural gas mixtures show a higher reactivity at lower temperatures due to the low-temperature chemistry pathways of the longer alkanes in these mixtures. The ignition delay times of the natural gas mixtures come closer to the ignition delay times of the hydrogen mixtures at higher temperatures.

Results from the Shock-Tube mixtures

Finally, the experiments from the shock-tube experiments were conducted, and the results are compared herein to the chemical kinetic model. A plot for each of the percentages of water (0%, 10% and 30%) was created at equivalence ratios of 2.0, 1.0, and 0.5; pressures of 1.6 atm, 11 atm, and 30 atm; and temperatures from 1478 K to 2103 K. The model calculations were performed assuming constant-volume conditions in a 0-D reactor. Since more than one parameter was changed between each of the shock-tube mixtures, it is difficult to compare one mixture to another. It is best instead to compare the model and experiment over this comprehensive range of data. Such comparisons are seen in Figs. 14 through 16. Three mixtures are plotted in each figure, with the common condition in each being the amount of water contained in the mixtures. As can be seen in the plots, the simulated ignition delay times compare very well with the shock-tube results over the entire range of conditions. They are typically within 10% of the measured times for most of the cases. However, they are up to 50% longer than measured at lower temperatures (1535 K) for the case with 10% water addition at phi = 0.5 and 11 atm, Fig. 15, and this decreases to 8% longer than measured to 1810 K. In the case of 30% water addition at φ = 0.5 and 11 atm, the predicted ignition delay times are longer than measured experimentally throughout the entire temperature range, being 40% longer at 1530 K reducing to 11% longer at 1870 K.

Conclusions

The aim of the present study was to investigate the influence of steam (water) on the ignition behavior of hydrogen, CO, and natural gas mixtures. To this end, experiments in a dual-piston rapid compression machine, complemented by kinetic simulations with the latest NUIG C_0–C_5 mechanism (AramcoMech 1.3) have been performed at 10 and 30 bar for equivalence ratios

of 0.5, 1.0, and 2.0. A matrix of nine different CH_4-O_2 mixtures and conditions was also studied behind reflected shock waves in a shock-tube facility for the same range of equivalence ratios as the RCM tests and for pressures between about 1 and 30 atm, all highly diluted in argon (98%). The shock-tube mixtures contained water at levels up to 30% of the fuel by volume. For all conditions, the kinetic model shows agreement well within the uncertainty of the experimental results. The major outcome is that only for the mixture with pure CO as the fuel does the addition of water to the initial mixture composition have a significant effect on ignition delay times. In this case, the water in the mixture allows for the formation of ȮH radicals which decrease ignition delay times, which is not possible with only CO as the fuel. For all other mixtures, the addition of up to 30% water with respect to the amount of fuel does not show any significant chemical effect. However, thermal properties such as heat capacity and thermal diffusivity are strongly influenced by the water addition and may have to be considered for real applications.

Acknowledgements

This work at NUIG was supported by Science Foundation Ireland under grant number [08/IN1./I2055]. The work at TAMU was supported by Rolls-Royce Canada under the direction of Dr. Gilles Bourque. We would like to thank Dr. Kuiwen Zhang and Dr. Ultan Burke for their help in preparing this manuscript.

References

[1] S. Gadde, J. Wu, A. Gulati, G. McQuiggan, B. Koestlin, B. Prade, ASME Turbo Expo 2006 GT2006-90970 (2006) 547–554.

[2] O. Bolland, H. Undrum, Adv. Environ. Res. 7 (2003) 901–911.

[3] A. J. Minchener, Fuel 84 (2005) 2222–2235.

[4] Y. Xu, G. Zang, H. Chen, B. Dou, C. Tan, Int. J. Hydrogen Energy 37 (2012) 11805–11814.

[5] C. T. Bowman, Proc. Combust. Inst. 24 (1992) 859–878.

[6] M. J. Prather, J. A. Logan, Proc. Combust. Inst. 25 (1994) 1513–1527.

[7] G. Maggio, G. Cacciola, Fuel 98 (2012) 111–123.

[8] European Environment Agency: Efficiency of conventional thermal electricity generation (ENER 019) – Assessment published April 2013 http://www.eea.europa.eu/data-and-maps/indicators/efficiency-of-conventional-thermal-electricity-generation-1/assessment

[9] https://www.scribd.com/doc/23697531/Dry-Low-NOx-Combustion-for-Gas-Turbines

[10] T. Heppenstall, Appl. Therm. Eng. 18 (1998) 837–846.

[11] P. Chiesa, S. Consonni, J. Eng. Gas Turb. Power 121 (1999) 295–305.

[12] E. S. Rubin, C. Chen, A. B. Rao, Energy Policy 35 (2007) 4444–4454.

[13] F. Wang, J. Chiou, Energ. Convers. Manage. 45 (2004) 15–26.

[14] S. Agarwal, S. S. Kachhwaha, R. S. Mishra, J. Sci. Ind. Res. India 70 (2011) 544–553.

[15] A. K. Das, C.-J. Sung, Y. Zhang, G. Mittal, Int. J. Hydrogen Energy 37 (2012) 6901–6911.

[16] R. Adnan, H. Masjuki, T. Mahlia, Energy 43 (2012) 416–426.

[17] B. Wang, H. Olivier, H. Grönig, Combust. Flame 133 (2003) 93–106.

[18] T. Le Cong, P. Dagaut, Energy Fuel 23 (2009) 725–734.

[19] L. Brett, J. MacNamara, P. Musch, J. Simmie, Combust. Flame 124 (2001) 326–329.

[20] S. M. Gallagher, H. J. Curran, W. K. Metcalfe, D. Healy, J. M. Simmie, G. Bourque, Combust. Flame 153 (2008) 316–333.

[21] J. Würmel, J. Simmie, Combust. Flame 141 (2005) 417–430.

[22] E. Petersen, R. Hanson, Shock Waves 10 (2001) 405–420.

[23] Morley Gaseq ver. 0.79 (2005) (http://www.c.morley.dsl.pipex.com/).

[24] C. J. Aul, W. K. Metcalfe, S. M. Burke, H. J. Curran, E. L. Petersen, Combust. Flame 160 (2013) 1153–1167.

[25] R. J. Lee, F. M. Rupley, J. A. Miller, "The Chemkin Thermodynamic Database," Sandia National Labs., Rept. SAND87-8215B, Albuquerque, NM, March 1990.

[26] E. L. Petersen, M. J. A. Rickard, M. W. Crofton, E. D. Abbey, M. J. Traum, D. M. Kalitan, Meas. Sci. Tech. 16 (2005) 1716–1729.

[27] E. L. Petersen, Combust. Sci. Tech. 181 (2009) 1123–1144.

[28] Chemkin Pro 15101, Reaction Design: San Diego (2010).

[29] http://www.nuigalway.ie/c3/Mechanism_release/frontmatter.html

[30] M. Ó Conaire, H. J. Curran, J. M. Simmie, W. J. Pitz, C. K. Westbrook, Int. J. Chem. Kinet. 36 (2004) 603–622.

[31] A. Kéromnès, W. K. Metcalfe, N. Donohoe, H. J. Curran, W. J. Pitz, Detailed chemical kinetic model for h2 and h2/co (syngas) mixtures at elevated pressure, 2011.

[32] A. Kéromnès, W. K. Metcalfe, K. A. Heufer, N. Donohoe, A. K. Das, C.-J. Sung, J. Herzler, C. Naumann, P. Griebel, O. Mathieu, M. C. Krejci, E. L. Petersen, W. J. Pitz, H. J. Curran, Combust. Flame 160 (2013) 995–1011.

[33] W. Lowry, J. de Vries, M. Krejci, E. Petersen, Z. Serinyel, W. Metcalfe, H. Curran, G. Bourque, J. Eng. Gas Turb. Power 133 (2011) Article Number: 091501 (9 pages).

[34] D. Healy, D. M. Kalitan, C. J. Aul, E. L. Petersen, G. Bourque, H. J. Curran, Energy Fuel 24 (2010) 1521–1528.

[35] W. K. Metcalfe, S. M. Burke, S. S. Ahmed, H. J. Curran, Int. J. Chem. Kinet. 45(10) (2013) 638–675.

[36] A. Laskin, H. Wang, C. Law, Int. J. Chem. Kinet. 32 (2000) 589–614.

[37] S. Davis, C. Law, H. Wang, Combust. Flame 119 (1999) 375–399.

[38] A. W. Jasper, J. A. Miller, S. J. Klippenstein, J. Phys. Chem. A 117 (2013) 12243–12255.

List if Tables:

List if Figures:

simulations, dotted lines correspond to open symbols, dashed lines to open/solid symbols, solid lines to solid symbols. The pure NG mixture simulations are dash-dot lines.

Figure 11: Comparison of mixtures C1–C3 for 10 and 30 bar at an equivalence ratio of φ = 1.0, black: 10 bar, red: 30 bar.

Figure 12: Reaction pathway analysis at 20% CO consumption (30 bar, 1050 K, ϕ = 1.0), Red: mixture C1 without water, Blue: mixture C2 with water, dashed lines: pathways producing OH radicals (mixture M4).

Figure 13: Comparison of all RCM mixtures at 30 bar and an equivalence ratio of 1.0 in air.

Figure 14: Experimental and predicted ignition delay times for CH_4/O_2/Argon mixtures diluted in 98% argon (vol.) from the shock-tube experiments with 0% water. ■ – φ = 0.5, p = 1.6 atm; ● – φ = 2.0, p = 11 atm; ▲– φ = 1.0, p = 30 atm. Lines are model simulations.

Figure 15: Experimental and predicted ignition delay times for CH_4/O_2/Argon mixtures diluted in 98% argon (vol.) from the shock-tube experiments with 10% water. ■ – φ = 1.0, p = 1.6 atm; ● – φ = 0.5, p = 11 atm; ▲ – φ = 2.0, p = 30 atm. Lines are model simulations.

Figure 16: Experimental and predicted ignition delay times for CH_4/O_2/Argon mixtures diluted in 98% argon (vol.) from the shock-tube experiments with 30% water. ■ – φ = 2.0, p = 1.6 atm; ● – φ = 1.0, p = 11 atm; ▲ – φ = 0.5, p = 30 atm. Lines are model simulations.

Table 1: Mixture compositions investigated in % molar volume, the natural gas mixture (NG) contains 81.25% CH_4, 10% C_2H_6, 5% C_3H_8, 2.5% C_4H_{10}, and 1.25% C_5H_{12}, and the syngas mixture (Syn) contains 25% CO, 50% H_2, and 25% H_2O.

Mixture	**Fuel Composition**
H1	100% H_2
H2	70% H_2 + 30% H_2O
N1	90% NG + 10% H_2O
N2	70% NG + 30% H_2O
N3	70% NG + 15% Syn +15% H_2O
C1	100% CO
C2	70% CO + 30% H_2O
C3	35% H_2 + 35% CO + 30% H_2O
Note: φ = 0.5, 1.0, 2.0; p = 10 and 30 bar	

Table 2: Populated L9 matrix with omission of fourth factor for the shock-tube experiments of ignition delay times of CH_4/O_2/Argon mixtures diluted in 98% Argon (molar %).

Test	φ	P (atm)	H_2O
1	0.5	1.6	0
2	0.5	11	10
3	0.5	30	30
4	1.0	1.6	10
5	1.0	11	30
6	1.0	30	0
7	2.0	1.6	30
8	2.0	11	0
9	2.0	30	10

Table 3: Properties of RCM gas mixtures for φ = 1, T = 850 K, diluent: 50% N_2 + 50% Ar.

	Conductivity k (J/m.K.s)	**Density ρ (Kg/m^3)**	**Heat capacity Cp (J/Kg.K)**	**Thermal Diffusivity k/ρ.Cp (m^{2}s^{-1})**
90% NG + 10% H_2O	0.0511	13.95	990.1	3.70×10^{-6}
70% NG + 30% H_2O	0.0517	13.8	1006.3	3.723×10^{-6}
Δ [%]	1.17	–1.08	1.65	6.1×10^{-1}
100% H_2	0.1000	12.08	1173.7	7.053×10^{-6}
70% H_2 + 30% H_2O	0.0977	11.52	1260.2	6.73×10^{-6}
Δ [%]	–2.30	–4.64	7.37	–4.59

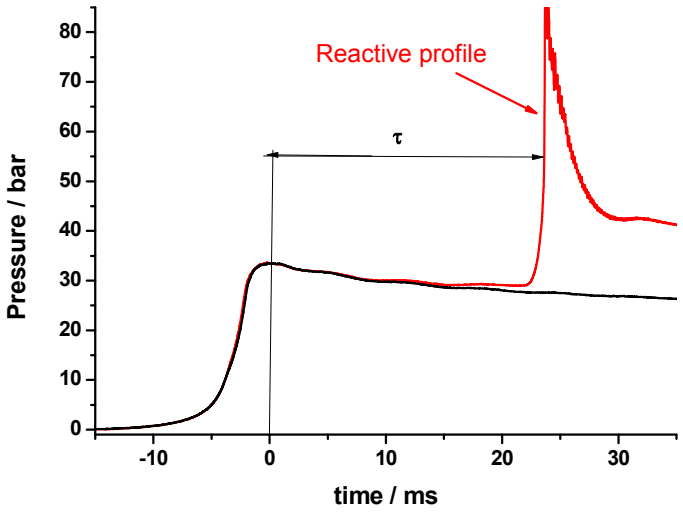

Figure 1: Sample of a reactive and a non-reactive pressure profile.

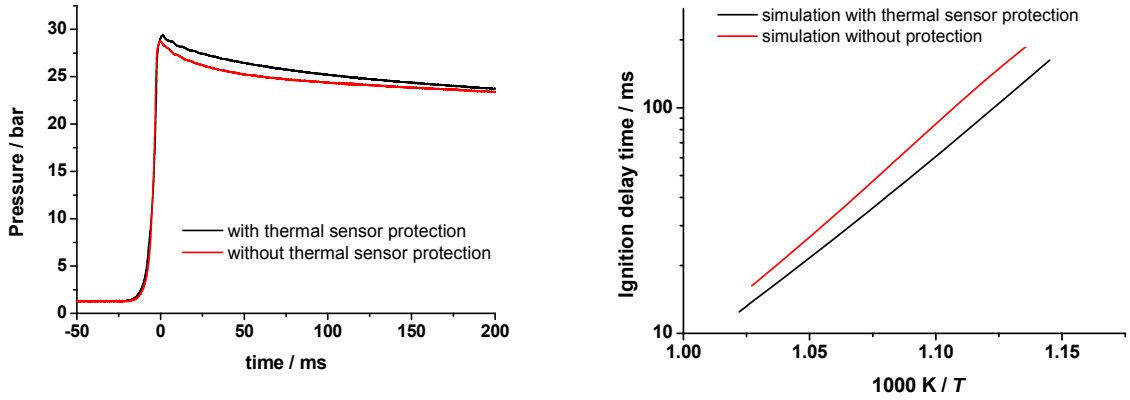

Figure 2: Results for 90% NG/10% H_2, φ = 2.0 in air. (a) Influence of thermal sensor protection on the pressure measurement in experiments and (b) Influence of different pressure profiles on simulation results.

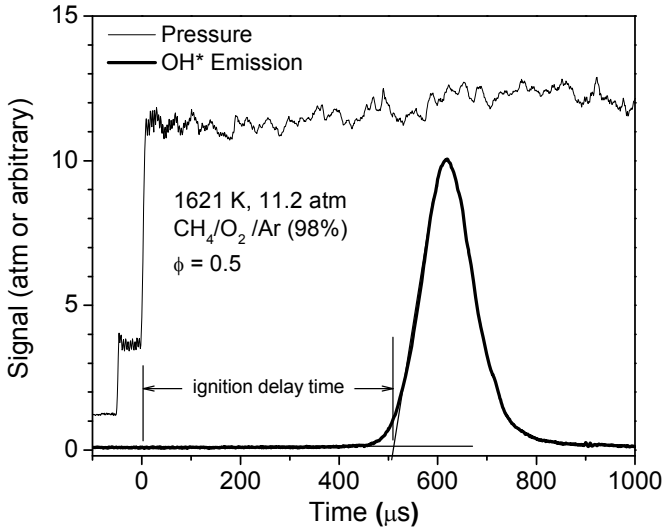

Figure 3: Sidewall Pressure and Sidewall OH* Emission obtained from the shock-tube experiment at 1621 K and 11.2 atm, showing the definition of ignition delay time form the OH* time history.

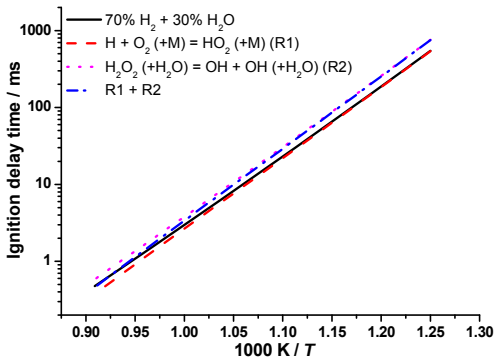

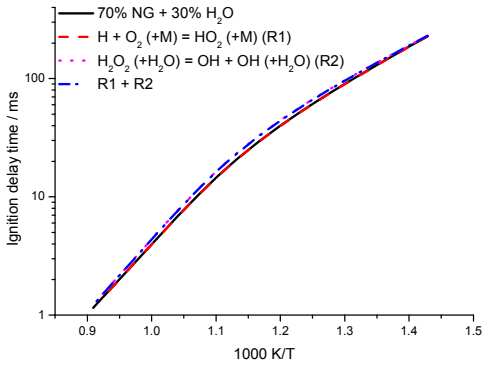

(a) 70% H_2 + 30% H_2O in air, φ = 1.0, p = 30 bar (b) 70% NG + 30% H_2O in air, φ = 1.0, p = 30 bar

Figure 4: Model predictions (adiabatic, constant volume) demonstrating the expected influence of water on the ignition delay time.

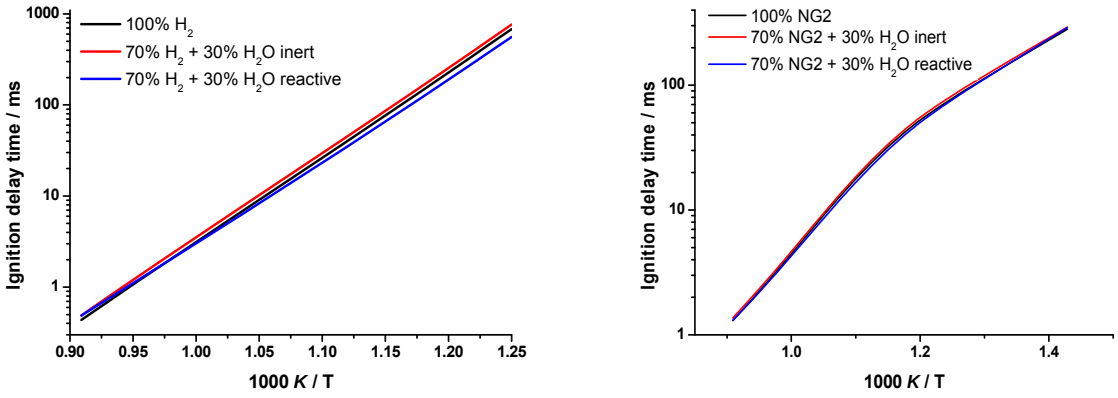

(a) (b)

Figure 5: Model predictions (adiabatic, constant volume) demonstrating the expected influence of water on the ignition delay time of (a) hydrogen and (b) natural gas in air at 30 bar.

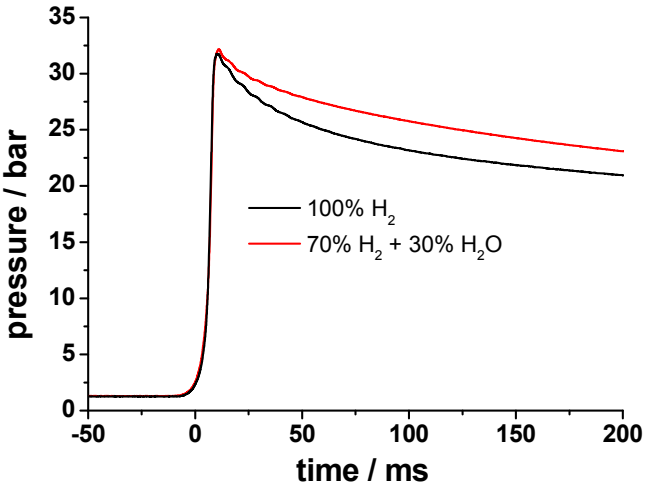

Figure 6: Influence of water concentration on the non-reactive pressure profiles for the mixtures H1 and H2.

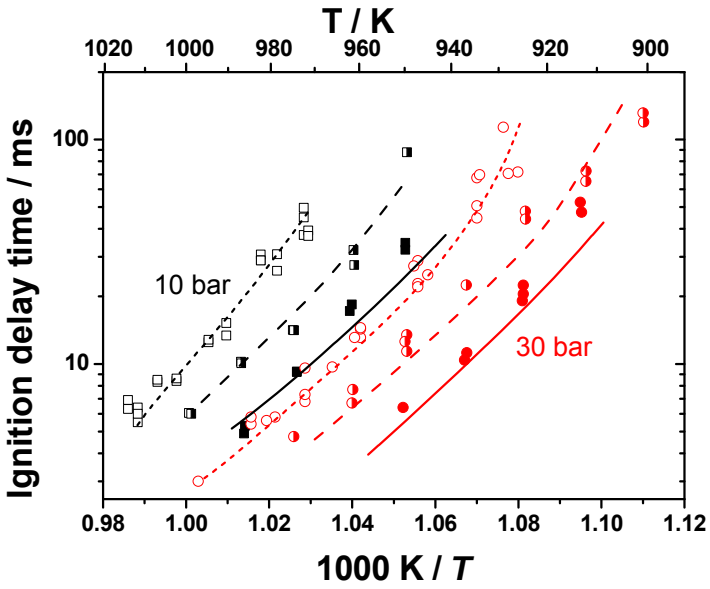

Figure 7: Ignition delay times for hydrogen at different pressures and equivalence ratios. □ – 10 bar, φ = 0.5, ◨ – 10 bar, φ = 1.0, ■ – 10 bar, φ = 2.0, ○ – 30 bar, φ = 0.5, ◑ – 30 bar, φ = 1.0, ● – 30 bar, φ = 2.0. Lines are model predictions; dotted lines correspond to open symbols, dashed lines to half-solid symbols, and solid lines to solid symbols.

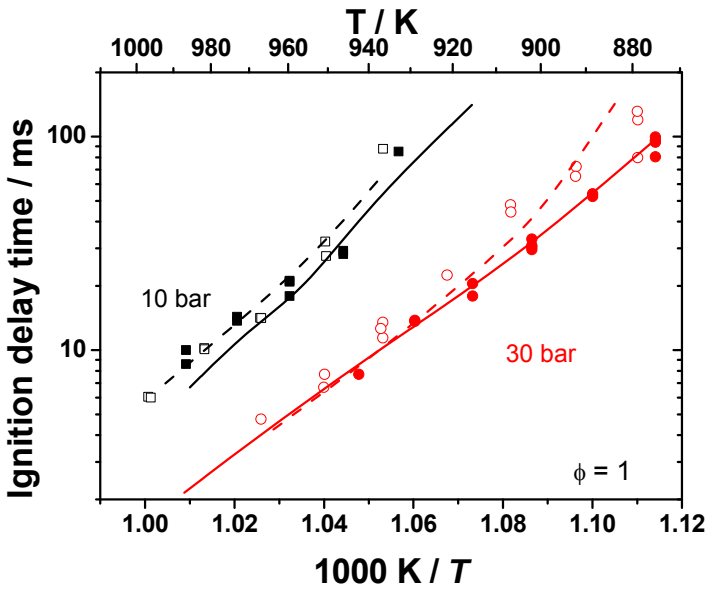

Figure 8: Experimental results for hydrogen + water. □ – 10 bar, 100% H_2, ■ – 10 bar, 70% H_2/30% H_2O, ○ – 30 bar, 100% H_2, ● – 30 bar, 70% H_2/30% H_2O. Lines are model simulation; solid lines correspond with solid symbols, dotted lines with open symbols.

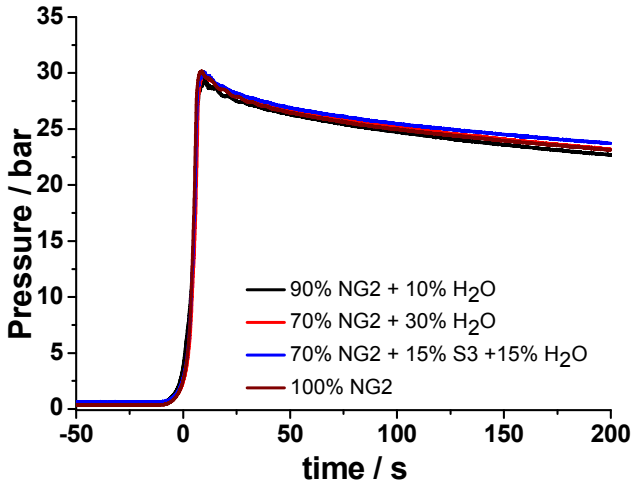

Figure 9: Influence of water concentration on the non-reactive pressure profiles for the mixtures N1–N3 and 100% NG.

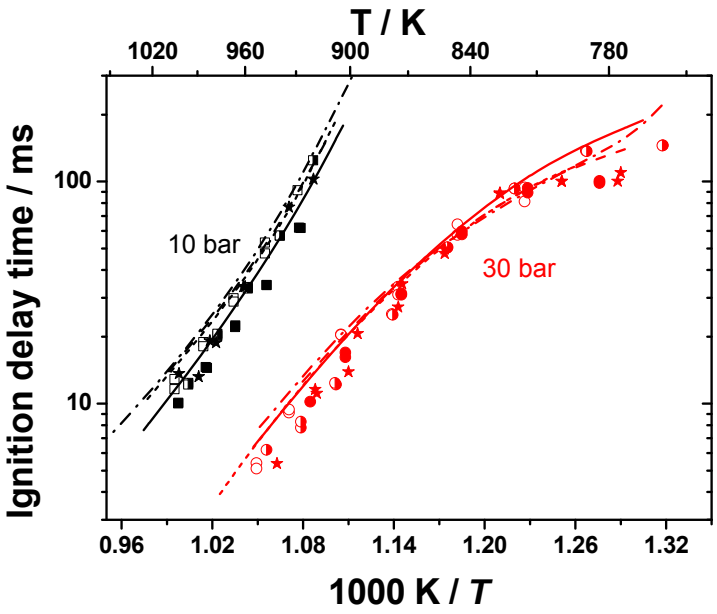

Figure 10: Experimental results for natural gas mixtures at φ = 1.0 in air in comparison to kinetic simulation. ⋆ NG, 10 bar, □ – mix N1, 10 bar, ◨ – mix N2, 10 bar, ■ – mix N3, 10 bar, ⋆ NG, 30 bar, ○ – mix N1, 30 bar, ◑ – mix N2, 30 bar, ● – mix N3, 30 bar. Lines are model simulations, dotted lines correspond to open symbols, dashed lines to open/solid symbols, solid lines to solid symbols. The pure NG mixture simulations are dash-dot lines.

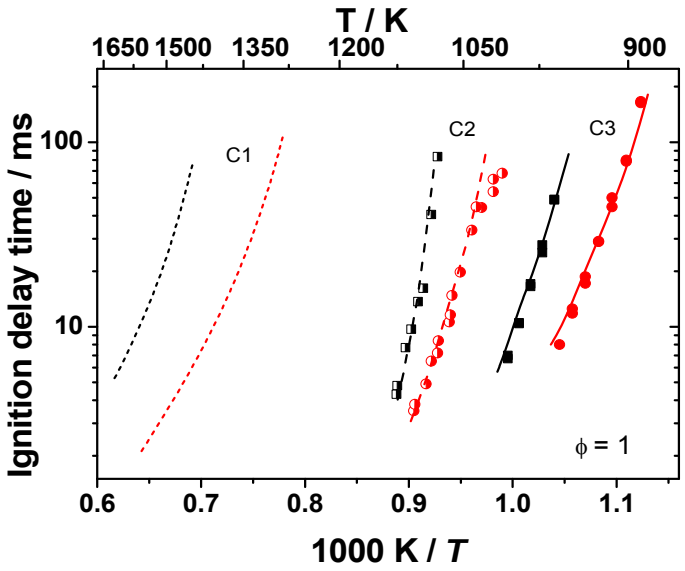

Figure 11: Comparison of mixtures C1–C3 for 10 and 30 bar at an equivalence ratio of φ = 1.0, black: 10 bar, red: 30 bar.

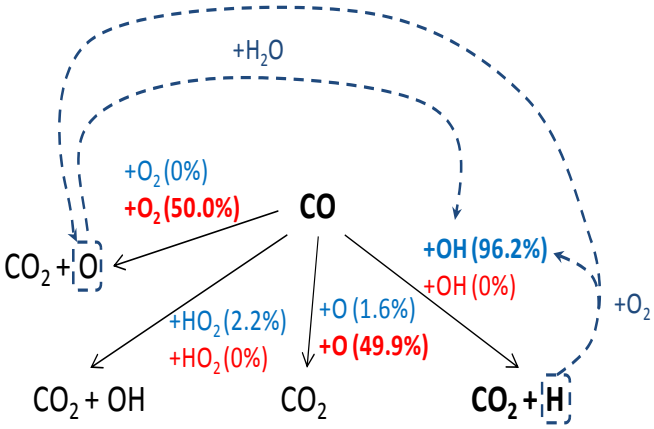

Figure 12: Reaction pathway analysis at 20% CO consumption (30 bar, 1050 K, ϕ = 1.0), Red: mixture C1 without water, Blue: mixture C2 with water, dashed lines: pathways producing OH radicals (mixture M4).

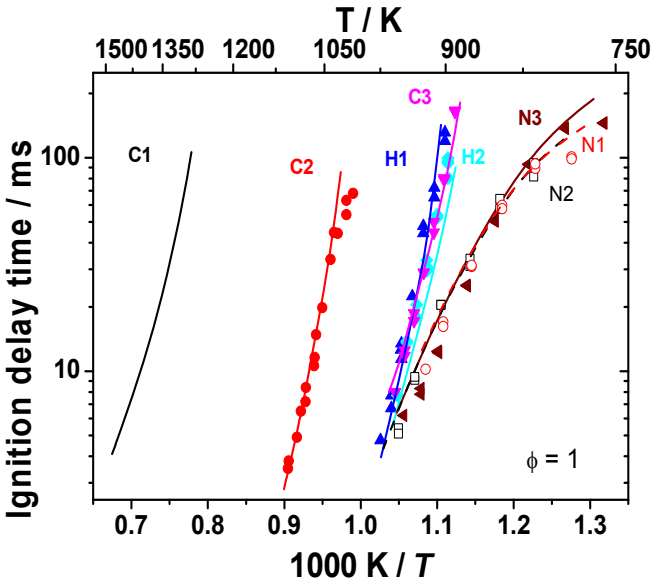

Figure 13: Comparison of all RCM mixtures at 30 bar and an equivalence ratio of 1.0 in air.

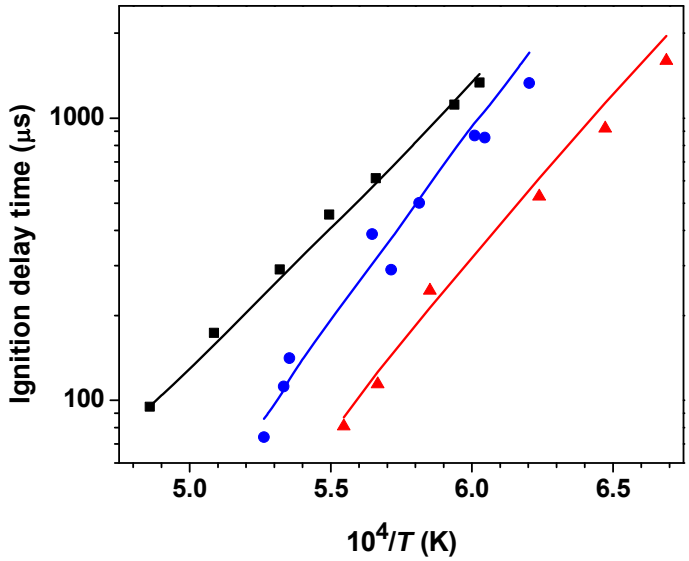

Figure 14: Experimental and predicted ignition delay times for CH_4/O_2/Argon mixtures diluted in 98% argon (vol.) from the shock-tube experiments with 0% water. ■ – φ = 0.5, p = 1.6 atm; ● – φ = 2.0, p = 11 atm; ▲ – φ = 1.0, p = 30 atm. Lines are model simulations.

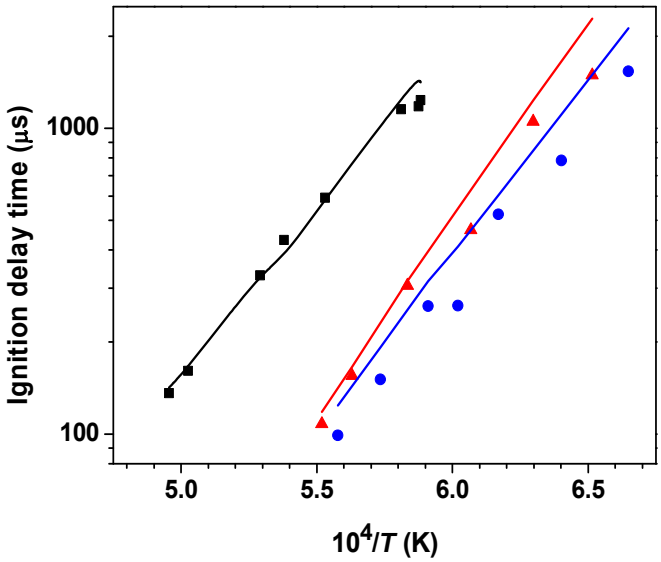

Figure 15: Experimental and predicted ignition delay times for CH_4/O_2/Argon mixtures diluted in 98% argon (vol.) from the shock-tube experiments with 10% water. ■ – φ = 1.0, p = 1.6 atm; ● – φ = 0.5, p = 11 atm; ▲ – φ = 2.0, p = 30 atm. Lines are model simulations.

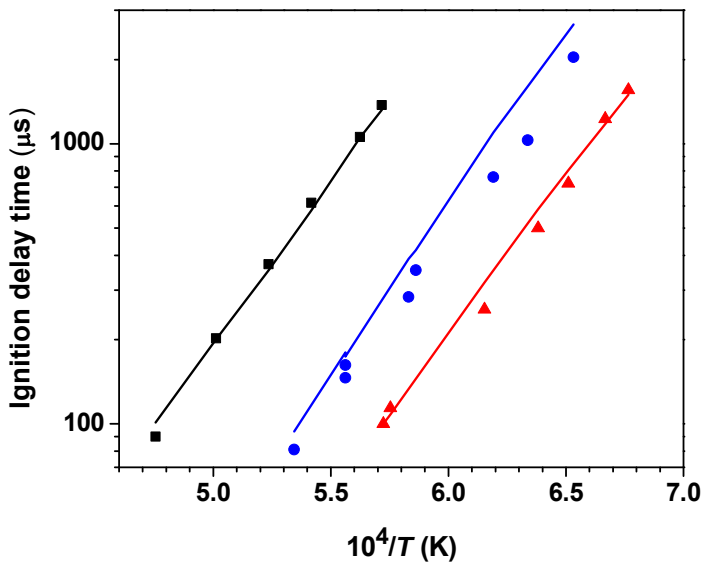

Figure 16: Experimental and predicted ignition delay times for CH_4/O_2/Argon mixtures diluted in 98% argon (vol.) from the shock-tube experiments with 30% water. ■ – φ = 2.0, p = 1.6 atm; ● – φ = 1.0, p = 11 atm; ▲ – φ = 0.5, p = 30 atm. Lines are model simulations.